Chapter 9

Atmospheric tides

Supplemental reading:

Chapman and Lindzen (1970)

Lindzen and Chapman (1969)

Lindzen (1979)

Lindzen (1967b)

One of the most straightforward and illuminating applications of internal gravity wave theory is the explanation of the atmosphere's tides. In any real problem we must adapt the theory to the specific problem at issue. *For tides, we must consider the following: 1. We are on an unbounded atmosphere; and 2. We are on a rotating sphere.*

By atmospheric tides we generally mean those planetary scale oscillations whose periods are integral fractions of a solar or lunar day (*diurnal* refers to a period of one day, *semidiurnal* refers to a period of half a day, and *terdiurnal* refers to a period of one third of a day). These periods are chosen because we know there is forcing at these periods. Gravitational forcing is precisely known; thermal forcing (due in large measure to the absorption of sunlight by O_3 and water vapor) is known with less precision. Nevertheless, a situation where forcing of known frequency is even reasonably well known is a situation of rare simplicity, and we may plausibly expect that our ability to calculate the observed response to such forcing constitutes a modest test of the utility of theory.

The situation was not always so simple. There follow sections on the history of this problem and on the observations of atmospheric tides. The history also provides a good example of what constitutes the 'scientific method' in an observational science where controlled experiments are not available.

9.1 History and the 'scientific method'

Textbooks in meteorology (and most other sciences) usually treat history (if they treat it at all) as an entertaining diversion from the 'meat' of a subject. I would hardly deny the fact that history is entertaining; however, I also happen to think that history is basic to the subject. In any field where there has been any success at all, one ought to see how significant problems were actually defined and solved (at least to the extent that they were defined and solved). From this point of view, this book actually devotes too little space to history. Thus, the present brief history of the study of atmospheric tides will have to serve as a surrogate for all the omitted histories of other topics we have covered. As such it is a relatively good choice. Just as atmospheric tides constitutes a relatively simple problem in dynamic meteorology, so too the history of this topic (at least until recently) has also been relatively easy to describe. To be sure a professional historian might balk at such a remark, but hopefully, the reader will be more indulgent of an amateur's approach. The history of the study of atmospheric tides provides a particularly good example of the form and pitfalls of the 'scientific method' in an observational science such as meteorology. Controlled experiments are generally out of the question. Instead, one begins with incompletely observed phenomena which are addressed by theoretical explanations. Explanations which go no further than dealing with the partial observations are more nearly simulations than theories, and given human nature, it is usually pretty certain that one will simulate pretty well what has been already observed. A theory should go further – it should offer predictions that go beyond the present observations so that the credibility of the theory can be tested as new observations are made. Quite properly, failure to confirm predictions tends to discredit theories, but confirmation does not as a rule rigorously establish the correctness of a theory; it merely increases our confidence in the theory. The process, in fact, can continue almost indefinitely, though at some point our confidence may seem so well founded that further tests will have a lower priority. The whole process is muddied by the fact that meteorological data

itself frequently is subject to substantial uncertainty. We will see examples of all these factors in the history of atmospheric tides.

In contrast to sea tides, which have been known and described for over two thousand years, atmospheric tides were not observed until the invention of the barometer by Torricelli (*ca.* 1643)[1]. Newton was able to explain the dominance of the lunar semidiurnal component of the sea tide. Briefly, tidal forcing depends not only on the average gravitational force exerted by either the sun or moon, but also on the relative variation of this force over the diameter of the earth. This latter factor gives a substantial advantage to the moon. The dominance of the semidiurnal component arises because, *relative* to the solid earth, the gravitational pull of the sun or moon or any other body simultaneously attracts the portion of the fluid shell directly under it and repels that portion of the envelope opposite it. From the perspective of the earth, both represent outward forces. (*viz* Figure 9.1. Thus, in a single

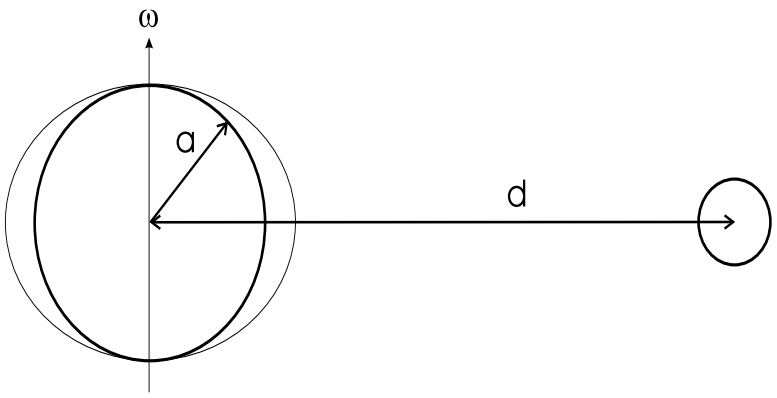

Figure 9.1: Schematic of gravitational tidal forcing

period of rotation the fluid envelope is pushed outward twice[2]. Newton already recognized that there ought to be a tidal response in the atmosphere as well as the sea, but he concluded that it would be too weak to be observed. Given seventeenth century data in Northern Europe, he was certainly correct. The situation is demonstrated in Figure 9.2, which shows time series for surface pressure at both Potsdam (52°N in Germany just outside of Berlin)

[1]Sea breezes, which marginally fit our definition of a tide, were undoubtedly observed earlier.

[2]For readers unfamiliar with sea tides, a simple treatment is provided in Lamb's (1916) classic treatise, *Hydrodynamics*.

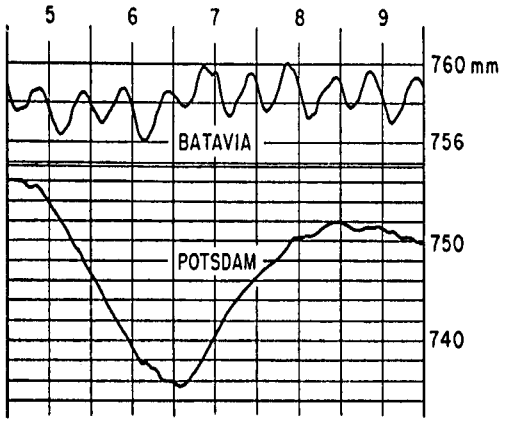

Figure 9.2: Barometric variations (on twofold different scales) at Batavia (6°S) and Potsdam (52°N) during November, 1919. After Bartels (1928).

and Batavia (6°S, the present day capitol of Indonesia, Jakarta). Clearly, whatever tiny tide that might exist at middle latitudes is swamped by large meteorological disturbances[3]. In the tropics, on the other hand, synoptic scale pressure perturbations are very small, while tidal oscillations are relatively large. The peculiar feature of these atmospheric surface pressure tides is that they are primarily solar semidiurnal. Laplace, already aware of this fact, concluded that the solar dominance implied a thermal origin.

It was Lord Kelvin (1882) who most clearly recognized the paradoxical character of these early observations. First, however, he confirmed the existing data by collecting and harmonically analyzing data from thiry stations for diurnal, semidiurnal, and terdiurnal components. The essence of the paradox is as follows: Gravitational tides are semidiurnal due to the intrinsic semidiurnal character of the forcing; if, however, atmospheric tides are thermally forced, then their forcing is predominantly diurnal. Why then is the response still predominantly semidiurnal? Kelvin put forward the hypothesis that the atmosphere had a free oscillation with zonal *wavenumber* 2 and a period near 12 hours which was resonantly excited by the small semidiurnal component of the thermal forcing. The reason that there is semidiurnal thermal forcing is simply that solar heating occurs only during approximately half

[3]Sidney Chapman's (1918) accurate determination of the lunar tide over England was an early triumph of signal detection.

the day. Thus the heating is not purely diurnal, and the harmonic distortion includes a significant semidiurnal component (*viz* Figure 9.3). This *resonance*

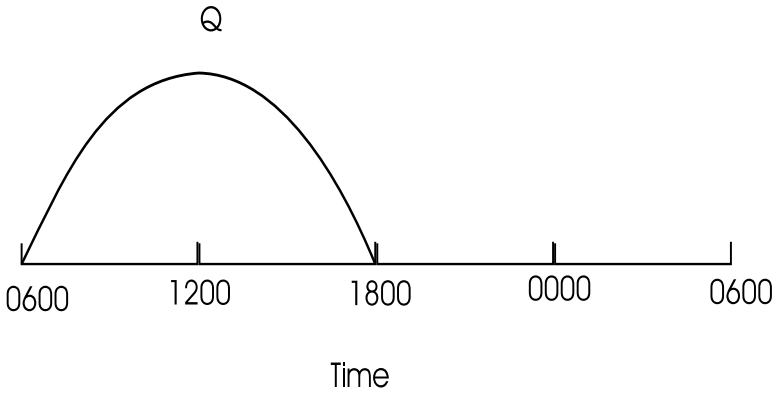

Figure 9.3: Schematic time dependence of solar forcing.

hypothesis dominated thinking on atmospheric tides for almost seventy years. Theoretical work centered on the search for the atmosphere's free oscillations. Following the terminology introduced in Section 8.7, Margules (1890) showed that an atmosphere with an *equivalent depth* of 7.85 km would, indeed, have a free oscillation of the required type. The atmosphere's equivalent depth depends on its thermal structure. In the late nineteenth century, this structure was largely unknown. However, both Rayleigh (1890) and Margules (1890, 1892, 1893), using very crude and unrealistic (in view of today's knowledge) assumptions, concluded that resonance was a possibility.

Lamb (1910, 1916) investigated the matter more systematically. He found that for either an isothermal basic state wherein density variations occur isothermally, or for an atmosphere with a basic state with an adiabatic lapse rate, the equivalent depth was very nearly resonant. Lamb also showed that when the basic state temperature varied linearly (but not adiabatically) with height, the atmosphere had an infinite number of equivalent depths – thus greatly increasing the possibility of resonance. Little note was taken of this result, but another suggestion of Lamb's was followed up: namely, his suggestion that the solar semidiurnal tide might, in fact, be gravitationally forced. His point was that such forcing would require such a degree of resonance to produce the observed tide that it would actually distinguish between the solar semidiurnal period and the lunar semidiurnal period (12 hr 26 min). The possibility of resonant selection is illustrated in Figure 9.4. Lamb, him-

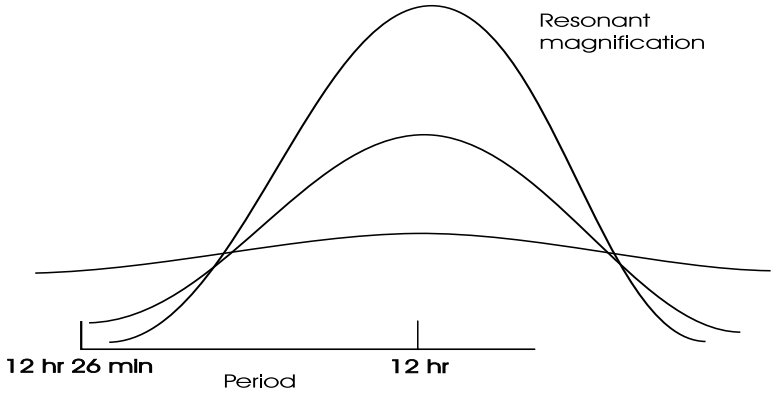

Figure 9.4: Schematic of resonant selection of solar semidiurnal tide.

self, noted at least two problems with this suggestion. First, of course, was the intrinsic unlikelihood of the atmosphere being so highly tuned. The second reason was that the phase of the observed surface pressure tide led rather than lagged the phase of the sun. This was opposite to what calculations showed. Chapman (1924) showed that the last item could be remedied if thermal forcing was of the same magnitude as gravitational forcing. With this rather coarse fix, the resonance theory was largely accepted for the next eight years. In terms of our discussion of scientific methodology, we were still, however, at the stage of simulation rather than theory. This situation changed dramatically with the work of Taylor and Pekeris.

In 1932, G.I. Taylor noted (as we saw in Section 8.7) that an atmosphere with an equivalent depth h would propagate small-scale disturbances (such as would be generated by explosions, earthquakes, etc.) at a speed $\sqrt{gh}$. Using data from the Krakatoa eruption of 1883[4], he showed that the atmospheric pulse travelled at a speed of $319\,\mathrm{ms}^{-1}$, corresponding to $h = 10.4\,\mathrm{km}$ — a value too far from 7.85 km to produce resonance. In 1936, Taylor returned to this problem, having rediscovered Lamb's earlier result that the atmosphere might have several equivalent depths. This allowed some hope for the, by now much modified, Kelvin resonance hypothesis. This hope received an immense boost from the work of Pekeris (1937).

Pekeris examined a variety of complicated basic states in order to see what distribution of temperature would support an equivalent depth of 7.85 km[5].

[4]Sometimes old data can serve in place of new data.

[5]This was an early form of inverse problem.

The distribution he found was one where the temperature decreased with height as observed in the troposphere; above the tropopause (*ca.* 12 km) the temperature increased with height to a high value (350°K) near 50 km, and then decreased upwards to a low value. It should be noted that in the mid–1930s we had no direct measurements of upper atmosphere temperature. However, independently of Pekeris, Martyn and Pulley (1936), on the basis of then recent meteor and anomalous sound data, proposed an observationally based thermal structure of the atmosphere which was in remarkable agreement with what Pekeris needed. It was almost as though Pekeris had deduced the atmosphere's complete thermal structure from tidal data at the earth's surface, simply by assuming resonance. His results, moreover, appeared to explain other observations of ionospheric and geomagnetic tidal variations. The vindication of the resonance theory seemed virtually complete. Pekeris countered Taylor's earlier criticism by showing that a low-level disturbance would primarily excite the faster mode associated with $h = 10.4$ km. A reexamination of the Krakatoa evidence by Pekeris even showed some evidence for the existence of the slower mode for which $h = 7.85$ km.

At this point a bit of editorial comment might be in order. If our story were to end at this point, it would have described a truly remarkable scientific achievement. In fact, as we shall soon see, the resonance theory proved to be profoundly wrong. The ability of Pekeris's theory to predict something well beyond the data that had motivated the theory did not end up proving the correctness of the theory! It will be useful to look at the remainder of this story to see where things fell apart. In some ways it is a fairly complicated story. However, before proceding, a few things should be noted concerning Pekeris's work. The explanation of the ionospheric and geomagnetic data did not (on subsequent scrutiny) actually depend on the resonance hypothesis. It is not, however, unheard of in science that one success is used to bolster another unrelated success. Similarly, Pekeris's reexamination of the Krakatoa data demonstrates the very real dangers relating to the analysis of ambiguous and noisy data by theoreticians with vested interests in the outcome of the analysis. Pekeris's claims for the data analysis were modest and circumspect, but even with the best will to be objective, he would have had difficulty not seeing at least hints of what he wanted to see. But all this is jumping ahead of our story. For fifteen years following Pekeris's remarkable work, most research on this subject was devoted to the refinement and interpretation of Pekeris's work. This research is comprehensively reviewed in a monograph by Wilkes (1949). Wilkes's monograph, incidentally, was the standard reference

on atmospheric oscillations for over a decade.

The first major objections to the resonance theory emerged in the aftermath of World War II when captured V2 rockets were used to probe the temperature structure of the atmosphere directly. The structure found differed from that proposed by Martyn and Pulley[6]. In particular, the temperature maximum at 50 km was much cooler (about 280°K rather than 350°K). In addition, the temperature decline above 50 km ended around 80 km, above which the temperature again increases, reaching very high values (600–1400°K) above 150 km. Jacchia and Kopal (1951), using an analog computer, investigated the resonance properties of the newly measured temperature profiles. They concluded that with the measured profiles, the atmosphere no longer had a second equivalent depth, and that the magnification of the solar semidiurnal tide was no longer sufficient to account for the observed semidiurnal tide on the basis of any realistic combination of gravitational excitation and excitation due to the upward diffusion of the daily variation of surface temperature[7]. As we shall see at the end of this chapter, Jacchia and Kopal were premature in claiming to have disproven the resonance theory; the real problems had not yet been identified. Nevertheless, their results were widely perceived as constituting the demise of resonance theory, and this perception fueled the search for additional sources of thermal forcing.

Although most of the sun's radiation is absorbed by the earth's surface, about 10 percent is absorbed directly by the atmosphere, and this appeared a likely source of excitation[8]. Siebert (1961) investigated the effectiveness of insolation absorption by water vapor in the troposphere, and found that it could account for one-third of the observed semidiurnal surface pressure oscillation. This was far more than could be accounted for by gravitational excitation or surface heating. Siebert also investigated the effectiveness of insolation absorption by ozone in the middle atmosphere. He concluded its effect was relatively small. We now know that this last conclusion is wrong.

[6]Here we see an example of a common phenomenon in meteorology: namely, data that turns out to not quite be data.

[7]Up to this point, this was the only form of thermal forcing considered.

[8]The absorptive properties of the atmosphere were actually sufficiently well known in the 1930s. It is curious that no one looked into their possible rôle in generating tides. Undoubtedly, the fact that the atmospheric sciences are actually a small field, and tides a small subset of a small field, played an important part. In addition specialization undeniably encourages a kind of tunnel vision.

In order to simplify calculations, Siebert used a basic temperature profile which was exceedingly unrealistic above the tropopause. As we shall see later in this chapter, this profile prevented the vertical propagation of semidiurnal tidal oscillations from the stratosphere to the troposphere. Butler and Small (1963) soon corrected this error, and showed that ozone absorption indeed accounted for the remaining two-thirds of the surface semidiurnal oscillation[9].

With a successful and robust theory in hand for the solar semidiurnal tide, we must return to Kelvin's seminal question: Why isn't the diurnal oscillation stronger than the semidiurnal? With the increased data available by the mid–1960s, even this question had become less obvious. Data above the ground up to about 100 km showed that at many levels and latitudes, the diurnal oscillations were as strong and often stronger than semidiurnal oscillations. Lindzen (1967) carried out theoretical calculations for the diurnal tide which provided satisfactory answers for the observed features. Central to the explanation is the fact that on half of the globe (polewards of $\pm 30^\circ$ latitude), 24 hr is longer than the local pendulum day (the period corresponding to the local Coriolis parameter), and under these circumstances a 24 hr oscillation is incapable of propagating vertically. We will explain this behaviour later in this chapter. In any event, because of this, it turns out that 80 percent of the diurnal forcing goes into physically trapped modes which cannot propagate disturbances forced aloft to the ground. The atmospheric response to these modes in the neighbourhood of the excitation is, however, substantial[10]. In addition, there exist (primarily equatorwards of $\pm 30^\circ$ latitude) diurnal modes which propagate vertically. However, as one could deduce from the dispersive properties of internal gravity waves (*viz.* Equation 8.55), the long period and the restricted latitude scale of these waves causes them to have relatively short vertical wavelengths (25 km or less). They are, therefore, subject to some destructive interference effects. Butler and Small suggested, in fact, that this could explain the relatively small amplitude of the diurnal tide, but subsequent calculations showed that

[9]In a rough sense, the work of Butler and Small completes our present understanding of the semidiurnal surface oscillation. However, as we shall see, the understanding is by no means complete. There is a discrepancy of about on hour in phase between theory and observation. There is also a problem with the predicted vertical structure of the tidal fields. Recent work suggests that these discrepancies are related to daily variations in rainfall.

[10]These trapped diurnal modes were discovered independently by Lindzen (1966) and Kato (1966).

this effect would be inadequate. What really proved to be important was that the propagating modes received only 20 percent of the excitation.

The story of tides hardly ends at this point. New data from the upper atmosphere continues to provide challenging questions. Tides still form an interesting focus for both observational and theoretical efforts. Still, after a century, Kelvin's question seems pretty much answered – for the moment.

9.2 Observations

Before proceeding to the mathematical theory of atmospheric tides, it is advisable for us to present a description of the phenomena about which we propose to theorize. As usual, our presentation of the data will be sketchy at best. The data problems discussed in Chapter 5 all apply here as well. Let it suffice to say that at many stages our observational picture is based on inadequate data; in almost all cases, the analyses of data have required the extrication of Fourier components from noisy data, and in some instances even the observational instruments have introduced uncertainties. Details of some of these matters may be found in Chapman and Lindzen (1970).

For many years, almost all data analyses for atmospheric tides were based on surface pressure data. Although tidal oscillations in surface pressure are generally small, at quite a few stations we have as much as 50–100 years of hourly or bi-hourly data. As a result, even today, our best tidal data are for surface pressure. Figures 9.5 and 9.6 show the amplitude and phase of the solar semidiurnal oscillation over the globe; they were prepared by Haurwitz (1956), on the basis of data from 296 stations[11]. The phase over most of the globe is relatively constant, implying the dominance of the migrating semidiurnal tide, but other components are found as well (the most significant of which is the semidiurnal standing oscillation for which $s = 0$; *viz.* Figure 9.7). If we let t =local time non-dimensionalized by the solar day, then, according to Haurwitz, the solar semidiurnal tide is well represented by:

$$\begin{aligned} S_2(p) = \quad & 1.16\ \sin^3\theta \sin(4\pi t + 158^\circ) \\ + \quad & 0.085\ P_2(\theta) \sin(4\pi t_u + 118^\circ)\ \text{mbar}, \end{aligned} \tag{9.1}$$

[11]It is tempting to seek more recent analyses, but since errors decrease only as the square root of the record length, the improvement so far is likely to be pretty negligible.

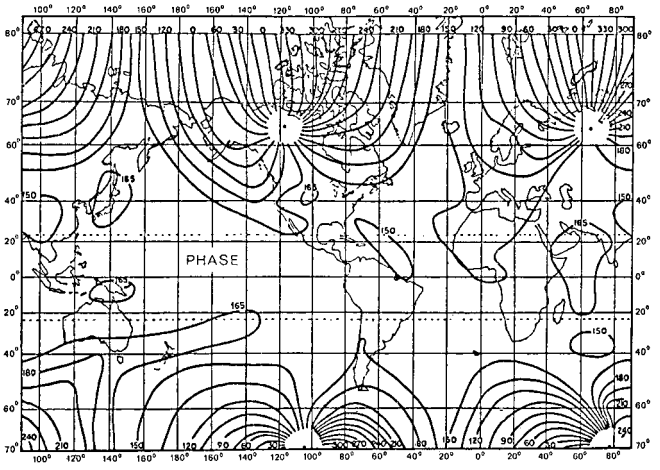

Figure 9.5: World maps showing equilines of phase (σ_2) of $S_2(p)$ relative to local mean time. After Haurwitz (1956).

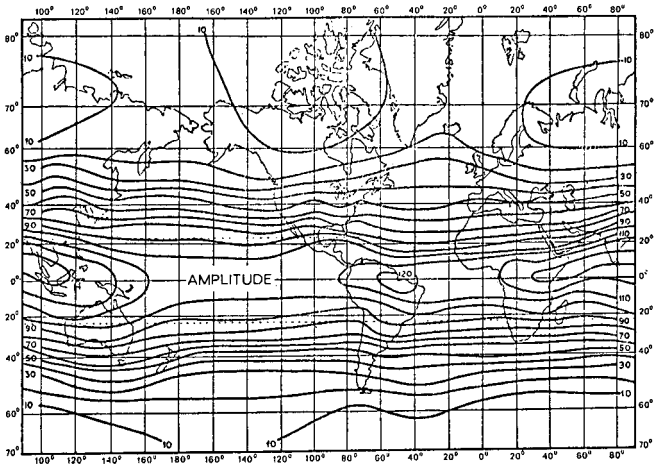

Figure 9.6: World maps showing equilines of amplitude (s_2, unit 10^{-2} mb) of $S_2(p)$. After Haurwitz (1956).

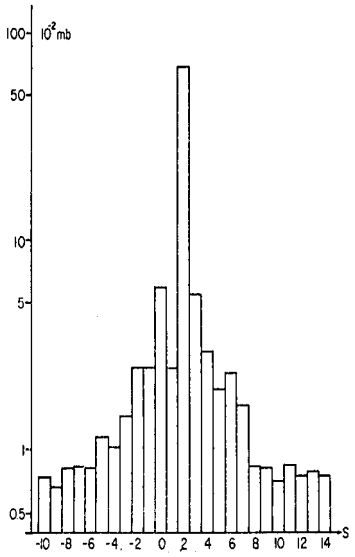

Figure 9.7: The amplitudes (on a logarithmic scale, and averaged over the latitudes 80°N to 70°S) of the semidiurnal pressure waves, parts of $S_2(p)$, of the type $\gamma_s \sin(2t_u + s\phi + \sigma_s)$, where t_u signifies universal mean solar time. After Kertz (1956).

where

$$\begin{aligned} \theta &= \text{colatitude} \\ t_u &= \text{Greenwich (Universal) time} \\ P_2(\theta) &= \frac{1}{2}(3\cos^2\theta - 1). \end{aligned}$$

One of the remarkable features of $S_2(p)$ is the fact that it hardly varies with season. This can be seen from Figure 9.8. The situation is more difficult for $S_1(p)$. It varies with season, it is weaker, and it is strongly polluted by non-migrating diurnal oscillations (*viz.* Figure 9.9). There are values of s with amplitudes as large as 1/4 of that pertaining to $s = 1$. (For $S_2(p)$, $s = 2$ was twenty times as large as its nearest competitor.) Moreover, large values of s, being associated with a small scale (large gradients), produce larger winds for a given amplitude of pressure oscillation than $s = 1$. We will return to this later. According to Haurwitz (1965), $S_1(p)$ is roughly representable as follows:

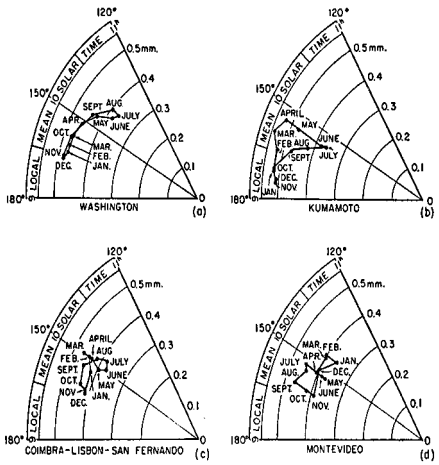

Figure 9.8: Harmonic dials showing the amplitude and phase of $S_2(p)$ for each calendar month for four widely spaced stations in middle latitudes, (a) Washington, D.C., (b) Kumamoto; (c) mean of Coimbra, Lisbon, and San Fernando; (d) Montevideo (Uruguay). After Chapman (1951).

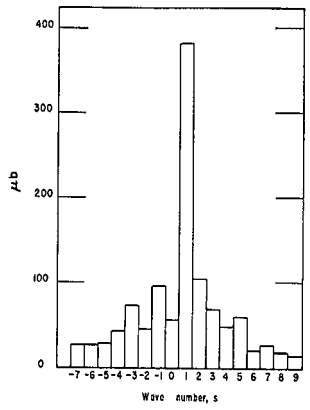

Figure 9.9: The amplitudes (averaged over the latitudes from the North Pole to 60°S) of the diurnal pressure waves, parts of $S_1(p)$, of the type $\gamma_s \sin(t_u + s\phi + \sigma_s)$. After Haurwitz (1965).

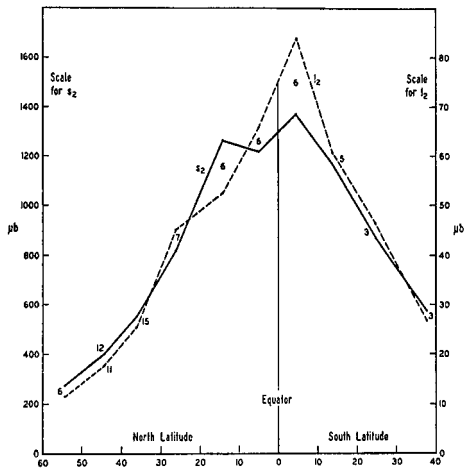

Figure 9.10: Mean values of the amplitude s_2 (full line) and l_2 (broken line) of the annual mean solar and lunar semidiurnal air-tides in barometric pressure, $S_2(p)$ and $L_2(p)$, for 10° belts of latitude. The numbers beside each point show from how many stations that point was determined. After Chapman and Westfold (1956).

$$S_1^1(p) = 593\ \sin^3\theta \sin(t + 12^\circ)\ \mu\text{bar}. \tag{9.2}$$

Data have also been analyzed for small terdiurnal and higher harmonics. Even $L_2(p)$ has been isolated. As we can see in Figure 9.10, the amplitude of $L_2(p)$ is about 1/20 of $S_2(p)$. $L_2(p)$ also has a peculiar seasonal variation, which can only be marginally discerned in Figure 9.11. The seasonal variation occurs with both the Northern and Southern Hemispheres in phase. This is much clearer in Figure 2L.2 in Chapman and Lindzen (1970), which summarizes lunar tidal data from 107 stations.

Data above the surface are rarer and less accurate, but some are available, with relatively recent radar techniques providing useful data well into the thermosphere.

At some radiosonde stations there are sufficiently frequent balloon ascents (four per day) to permit tidal analyses for both diurnal and semidiurnal components from the ground up to about 10 mb. Early analyses based on such data at a few isolated stations (Harris, Finger, and Teweles, 1962) were unable to distinguish migrating from non-migrating tides, but did establish orders of magnitude. Typically, horizontal wind oscillations were found to have amplitudes $\sim$ 10 cm/sec in the troposphere and $\sim$ 50 cm/sec in the

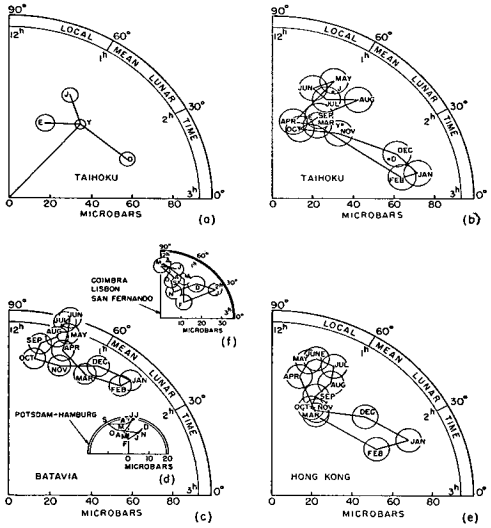

Figure 9.11: Harmonic dials, with probable error circles, indicating the changes of the lunar semidiurnal air-tide in barometric pressure in the course of a year. (a) Annual (y) and four-monthly seasonal (*j, e, d*) determinations for Taihoku, Formosa (now Taipei, Taiwan) (1897–1932). Also five sets of twelve- monthly mean dial points. After Chapman (1951).

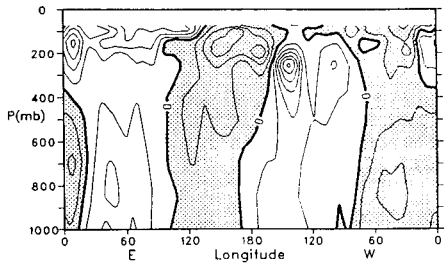

Figure 9.12: Semidiurnal zonal wind field for DJF 1986/87 along the equator; contour interval 0.2 m/sec. Regions of negative values are shaded. After Hsu and Hoskins (1989).

stratosphere. Global pictures of the behaviour of diurnal tides in horizontal wind, based on radiosonde data, were obtained by Wallace and Hartranft (1969) and Wallace and Tadd (1974) using the clever premise that the time average of the difference between wind soundings at 0000 UT and 1200 UT should represent a snapshot of the odd harmonics of the daily variation which are strongly dominated by the diurnal component. Recently, Hsu and Hoskins (1989) have shown that analyzed ECMWF (European Centre for Medium-range Weather Forcasting) data successfully depict diurnal and semidiurnal tides below 50 mb (the upper limit of ECMWF analyses). Their results for the semidiurnal oscillation in zonal wind along the equator are shown in Figure 9.12. We see a clear wavenumber 2 pattern indicative of a migrating tide. We also see very little tilt with height. The diurnal oscillations are more complicated. Figure 9.13 shows a snapshot of the diurnal component of the height field along the equator at 0000 GMT averaged over the winter of 1986/87. There is a clear wavenumber 1 pattern with some evidence of phase tilt. However, the distortion from a strict sine wave has important consequences for the diurnal wind pattern (Why?). This becomes evident in Figure 9.14 which shows a comparably averaged snapshot of the diurnal component of the horizontal wind at 850 mb. The pattern is more complicated; wavenumber 1 is no longer self-evidently dominant. There are numerous regional diurnal circulations. Figure 9.15 shows a similar snapshot at 50 mb; regional features are still evident but less pronounced. As already noted, ECMWF analyses do not extend beyond 50 mb. However, a similar snapshot from Wallace and Hartranft (1969) for 15 mb (involving, however, an annual rather than a winter average), shown in Figure 9.16, does suggest

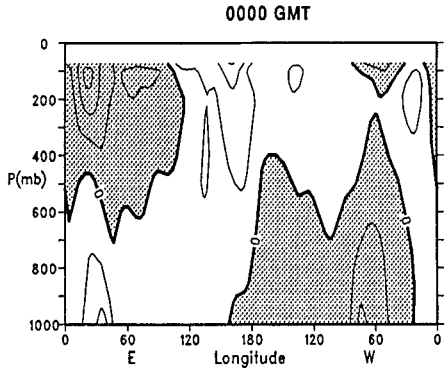

Figure 9.13: Vertical cross section of the diurnal height field along the equator at 0000 GMT in DJF 1986/87. Contour interval is 5 m. Regions of negative values are shaded. After Hsu and Hoskins (1989).

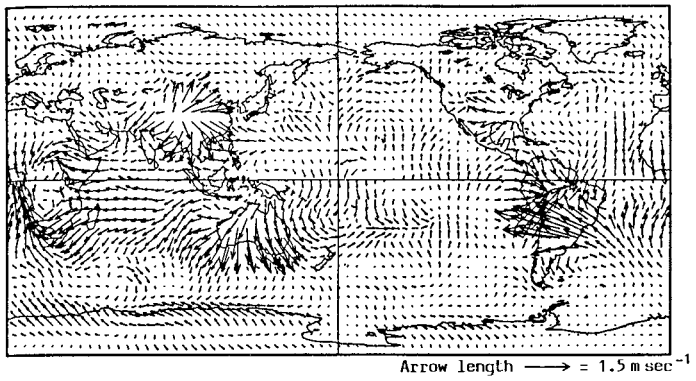

Figure 9.14: The diurnal wind vectors in DJF 1986/87 at 850 mb at 0000 GMT. After Hsu and Hoskins (1989).

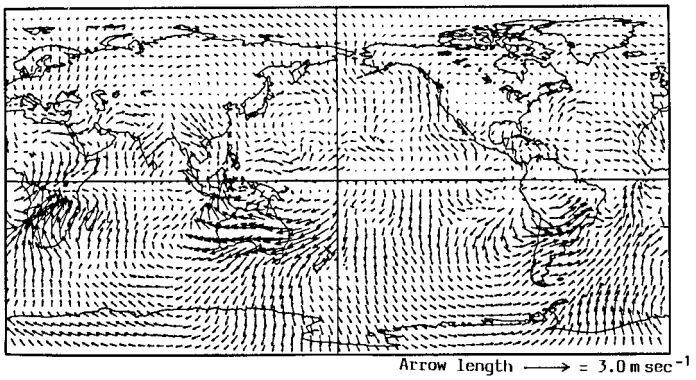

Figure 9.15: The diurnal wind vectors in DJF 1986/87 at 50 mb at 0000 GMT. After Hsu and Hoskins (1989).

Figure 9.16: Annual average wind differences 0000–1200 GMT at 15 mb plotted in vector form. The length scale is given in the figure. After Wallace and Hartranft, (1969).

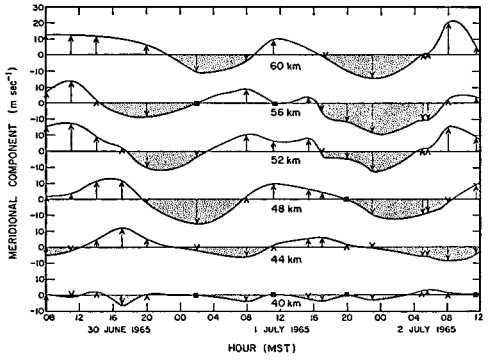

Figure 9.17: Meridional wind component, u, in m/sec averaged over 4 km centred at 40, 44, 48, 52, 56, and 60 km. Positive values indicate a south to north flow. After Beyers, Miers, and Reed (1966).

a wavenumber 1 dominance (characterized by flow over the pole; why?). The data up to 15 mb offer some reason to expect that the regional influences die out within the lower stratosphere, and that above 15 mb, diurnal oscillations are mostly migrating.

In the region between 30 and 60 km, most of our data come from meteorological rocket soundings. These are comparatively infrequent and the method of analysis becomes *a priori*, a serious problem. However, it turns out that results of different analyses appear to be compatible (at least for the diurnal component) because tidal winds at these heights are already a very significant part of the total wind (at least in the north-south direction).

This is seen in Figure 9.17, where we show the southerly wind as measured over a period of 51 h at White Sands, N.M. Analyses of tidal waves at various latitudes are now available. Figure 9.18 shows the phase and amplitude of the semidiurnal oscillation at about 30°N. Below 50 km, the results appear quite uncertain (Reed, 1967). In Figures 9.19 and 9.20 we see the diurnal component at 61°N and at 20°N, respectively. Amplitudes are of the order of 10 m sec^{-1} at 60 km but phase at 20°N is more variable than at 61°N (Reed, Oard, and Siemanski, 1969).

Between 60 km and 80 km, there are too few data for tidal analyses. Between 80 and 105 km, there is a growing body of data from the observation of ionized meteor trails by Doppler radar. The earliest such data were for vertically averaged wind over the whole range 80–105 km. Some such data for Jodrell Bank (Greenhow and Neufeld, 196l) (58 °N) and Adelaide

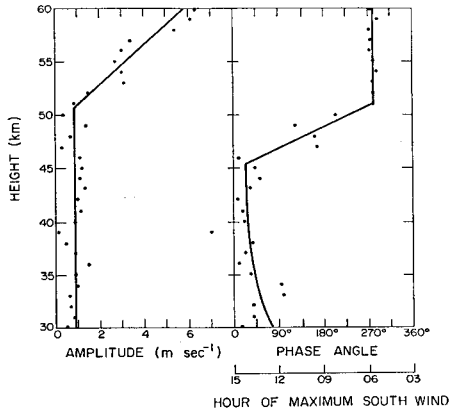

Figure 9.18: Phase and amplitude of the semidiurnal variation of the meridional wind component u at 30°N based on data from White Sands (32.4°N) and Cape Kennedy (28.5°N). After Reed (1967).

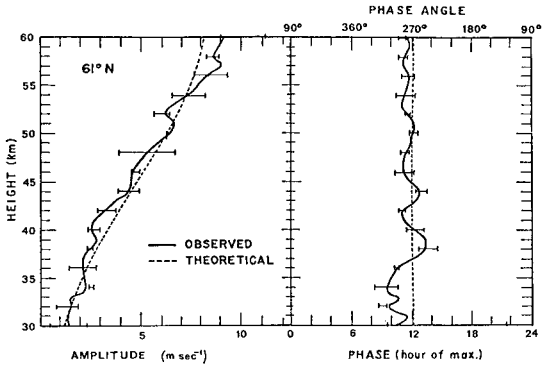

Figure 9.19: Phase and amplitude of the diurnal variation of the meridional wind component u at 61°N. Phase angle, in accordance with the usual convention, gives the degrees in advance of the origin (chosen as midnight) at which the sine curve crosses from $-$ to $+$. The theoretical curves will be discussed later in this chapter. After Reed, *et al.* (1969).

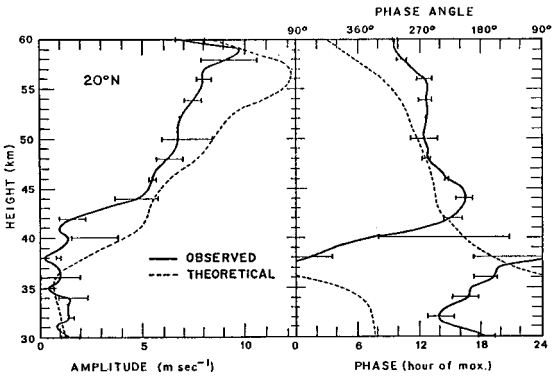

Figure 9.20: Phase and amplitude of the diurnal variation of the meridional wind component u at 20°N. Phase angle, in accordance with the usual convention, gives the degrees in advance of the origin (chosen as midnight) at which the sine curve crosses from $-$ to $+$. The theoretical curves will be discussed later in this chapter. After Reed, *et al.* (1969).

(Elford, 1959) (35 °S) showed typical magnitudes of around 20 m sec^{-1}. All quantities were subject to large seasonal fluctuations and error circles. At Adelaide, diurnal oscillations predominated, whereas at Jordell Bank semidiurnal oscillations predominated; at both stations tidal winds appeared to exceed other winds. The extensive vertical averaging made it difficult to compare these observations with theory. Improvements in meteor radars have made it possible to delineate horizontal winds with vertical resolutions of 1–2 km over the height range 80 to 105 km. Such results are reviewed in Glass and Spizzichino (1974). Typical amplitudes and phases for semidiurnal and diurnal tides obtained by this technique over Garchy, France are shown in Figure 9.21. The semidiurnal phase variation with height is substantially greater than is typically seen at lower altitudes. The diurnal tide at this location is typically weaker than the semidiurnal tide; it is also usually associated with much shorter vertical wavelengths.

Between 90 and 130 km (and higher), wind data can be obtained by visually tracking luminous vapor trails emitted from rockets. In most cases this is possible only in twilight at sunrise and sundown. Hines (1966) used such data to form twelve-hour wind differences, which seemed likely to indicate the diurnal contribution to the total wind at dawn at Wallops Island (38°N). Hines assumed that the average of the winds measured twelve hours apart would be due to the sum of prevailing and semidiurnal winds. His results are shown in Figure 9.22. There is an evident rotation of the diurnal

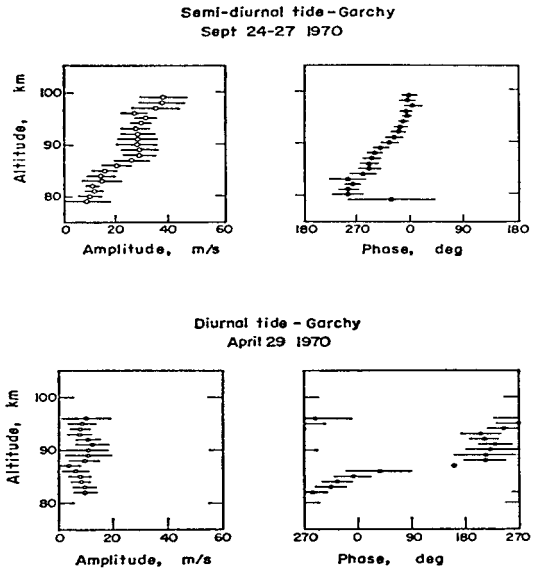

Figure 9.21: Amplitude and phase of the semidiurnal component of the eastward velocity over Garchy observed by meteor radar during September 24–27, 1970 (top), and of the diurnal component during April 29, 1970 (bottom). After Glass and Spizzichino (1974).

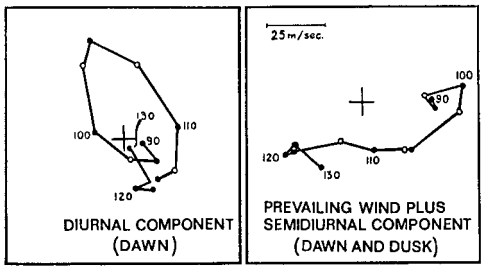

Figure 9.22: Vector diagrams showing (a) the diurnal tide at dawn and (b) the prevailing wind plus the semidiurnal tide at its dawn-dusk phase, as functions of height. The data used were from both Wallops Island, Virginia, and from Sardinia (both near 38°N). After Hines (1966).

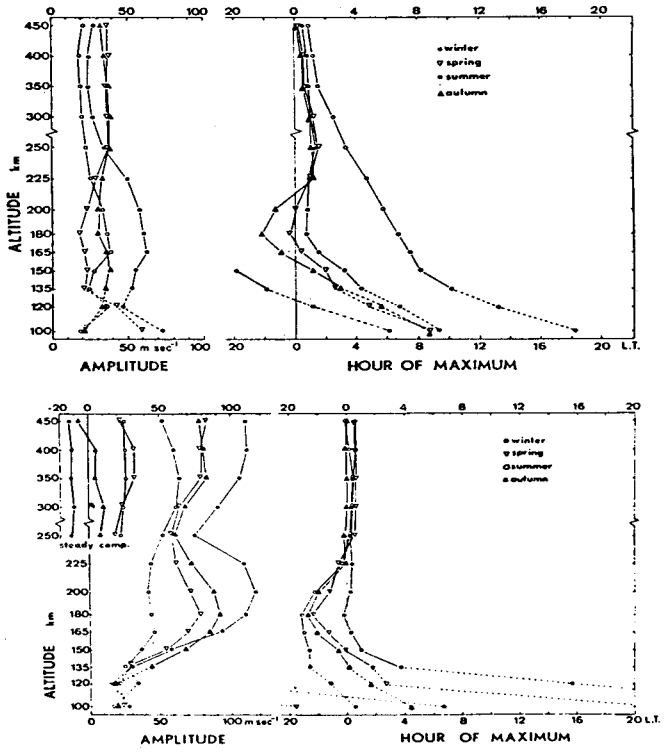

Figure 9.23: Mean seasonal vertical structures of amplitude and phase of the southward neutral wind from 1971–2 observations at St. Santin (45°N). (*top*) Semidiurnal component; (*bottom*) Steady and diurnal components. After Amayenc (1974).

wind vector with height, characteristic of an internal wave with a vertical wavelength of about 20 km. Amplitude appears to grow with height up to 105 km, and then to decay.

Over the past twenty years, it has become possible to observe the atmosphere both in the mesosphere and above 100 km in considerable detail using the incoherent backscatter of powerful radar signals. Figure 9.23 shows tidal amplitudes and phases obtained for altitudes between 100 and 450 km over St. Santin, France (45°N). Above 150 km we see that the diurnal component is again dominant; also, above about 225 km all amplitudes and phases are almost independent of height. Finally, it should be noted that the amplitudes are very large ($\sim$ 100 m/s for the diurnal component). The temperature oscillations have comparable amplitudes ($\sim$ 100 K).

Before proceeding to the mathematical theory, it may be helpful to sum-

marize the observations.
The situation for surface pressure is fairly straightforward. S2(p)∼ 1mb with maxima at 0940 and 2140; S1(p)∼ 0.6mb with a maximum at 2312; and L2(p)∼ .08mb with maxima 1020 and 2220 lunar time In addition, S1 is quite variable and irregular, S2 is stable, and L2 is somewhat seasonally variable with global seasonality.
The situation higher up is more complex:
The diurnal tide in horizontal wind is stronger in stratosphere. Also, there is more phase variation with altitude at lower latitudes than at high latitudes.
There is something of a gap in data between 60 and 80 km.
In mesosphere and lower thermosphere, the semidiurnal tide in horizontal wind appears stronger at higher latitudes while the diurnal tide seems to dominate at lower latitudes.
In the thermosphere, results seem to depend on solar activity.

9.3 Theory

We will restrict ourselves to 'migrating tides' whose dependence on time and longitude is given by $e^{2\pi i s t_\ell}$ where t_ℓ = local time in days. $t_\ell = t_u + \phi/2\pi$, where ϕ is longitude and t_u = universal time. We will generally refer to t_u simply as t. $s = 1$ corresponds to a diurnal tide; $s = 2$ refers to a semidiurnal tide, and so forth. Such oscillations have phase speeds equal to the linear rotation speed of the earth. Since this speed is generally much larger than typical flow speeds we usually assume the basic state to be static. Also the periods are sufficiently long to allow us to use the hydrostatic approximation. This, in turn, allows us to replace z as a vertical coordinate with

$$z^* \equiv -\ln\left(\frac{p}{p_s}\right). \tag{9.3}$$

(Recall $p = p_s e^{-z^*}$, where $z^* = \int_0^z \frac{dz}{H}$, $H = \frac{RT_0}{g}$). This coordinate system (log–pressure) is described in Holton. The resulting equations no longer formally include density, and, as a result, they are virtually identical to the Boussinesq equations without, however, the same restrictions. In this coordinate system vertical velocity is replaced by

$$w^* = \frac{dz^*}{dt} = -\frac{1}{p}\frac{dp}{dt} \tag{9.4}$$

and pressure is replaced by geopotential

$$\Phi = gz(z^*).$$

The only (minor) difficulty with this scheme is that the lower boundary condition is that

$$w = 0 \text{ at } z = 0 \tag{9.5}$$

and w^* is *not* the vertical velocity.

The correct lower boundary condition in log – p coordinates is obtained as follows:

At $z = z^* = 0,\ w = 0$, so that

$$w^* = -\frac{1}{p_s}\frac{dp'}{dt} = -\frac{1}{p_s}\left(\frac{\partial p'}{\partial t} + w'\frac{dp_0}{dz}\right) = -\frac{1}{p_s}\frac{\partial p'}{\partial t}.$$

From $dp = \frac{\partial p}{\partial t}dt + \cdots + \frac{\partial p}{\partial z}dz$ we get

$$\left(\frac{\partial z}{\partial t}\right)_p = -\frac{\frac{\partial p'}{\partial t}}{\frac{\partial p}{\partial z}} = \frac{\frac{\partial p'}{\partial t}}{\rho g}$$

or

$$\frac{\partial p'}{\partial t} = \rho\frac{\partial \Phi}{\partial t}.$$

Thus

$$w^* = -\frac{\rho_s}{p_s}\frac{\partial \Phi}{\partial t} = -\frac{1}{gH(0)}\frac{\partial \Phi'}{\partial t} \text{ at } z^* = 0. \tag{9.6}$$

Equation 9.6 is our appropriate lower boundary condition.

It is, unfortunately, the case that tidal theory has used different horizontal coordinates than those used in the rest of meteorology; θ = colatitude, ϕ = longitude, u = northerly velocity, and v = westerly velocity. Assuming time and longitude dependence of the form $e^{i(\sigma t + s\phi)}$ (somewhat more general than our earlier choice) our linearized equations for horizontal motion are simply

$$i\sigma u' - 2\Omega \cos\theta v' = -\frac{1}{a}\frac{\partial}{\partial\theta}\Phi' \tag{9.7}$$

and

$$i\sigma v' + 2\Omega \cos\theta u' = -\frac{is}{a\sin\theta}\Phi'. \tag{9.8}$$

The hydrostatic relation becomes

$$\frac{\partial\Phi'}{\partial z^*} = RT'. \tag{9.9}$$

Continuity becomes

$$\nabla\cdot\vec{u}_{hor} + \frac{\partial w^*}{\partial z^*} - w^* = 0 \tag{9.10}$$

(The correction to the Boussinesq expression is due to the fact that our fluid can extend over heights larger than a scale height.), and the energy equation becomes

$$i\sigma T' + w^*(\frac{dT_0}{dz^*} + \frac{RT_0}{c_p}) = \frac{J}{c_p}. \tag{9.11}$$

(N.B. $\frac{dT_0}{dz^*} + \frac{RT_0}{c_p} = H(\frac{dT_0}{dz} + \frac{g}{c_p})$.) *The fact that the hydrostatic equations in log p coordinates look almost exactly like the Boussinesq equations is, perhaps, the most important justification for the Boussinesq approximation.*
Equation 9.9 allows us to immediately eliminate T' from Equation 9.11:

$$i\sigma\frac{\partial\Phi}{\partial z^*} + w^* R\left(\frac{dT_0}{dz^*} + \frac{RT_0}{c_p}\right) = \kappa J. \tag{9.12}$$

The procedure used in solving Equations 9.7, 9.8, 9.10, and 9.12 is sufficiently general in utility to warrant sketching here.

We first note that Equations 9.7 and 9.8 are simply algebraic equations in u' and v' which are trivially solved:

$$u' = \frac{i\sigma}{4a^2\Omega^2(f^2 - \cos^2\theta)}\left(\frac{\partial}{\partial\theta} + \frac{s\cot\theta}{f}\right)\Phi' \tag{9.13}$$

and

$$v' = \frac{-\sigma}{4a^2\Omega^2(f^2 - \cos^2\theta)} \left(\frac{\cos\theta}{f} \frac{\partial}{\partial\theta} + \frac{s}{\sin\theta} \right) \Phi', \tag{9.14}$$

where

$$f \equiv \sigma/2\Omega.$$

Now u' and v' (and all information about rotation and sphericity) enter the remaining two equations only through $\nabla \cdot \vec{u}_{hor}$ in Equation 9.10. Using Equations 9.13 and 9.14 we may express $\nabla \cdot \vec{u}_{hor}$ as follows:

$$\nabla \cdot \vec{u}_{hor} = \frac{1}{a\sin\theta} \frac{\partial}{\partial\theta}(u'\sin\theta) + \frac{1}{a\sin\theta} isv' \tag{9.15}$$

$$= \frac{i\sigma}{4a^2\Omega^2} F[\Phi'], \tag{9.16}$$

where

$$F \equiv \left\{ \frac{1}{\sin\theta} \frac{\partial}{\partial\theta} \left(\frac{\sin\theta}{f - \cos^2\theta} \frac{\partial}{\partial\theta} \right) - \frac{1}{f^2 - \cos^2\theta} \left(\frac{s}{f} \frac{f^2 + \cos^2\theta}{f^2 - \cos^2\theta} + \frac{s^2}{\sin^2\theta} \right) \right\} \Phi'. \tag{9.17}$$

9.3.1 Laplace's tidal equation

Note that apart from F, Equations 9.10 and 9.12 depend only on z^*. We can make the present problem almost identical to the problem in Section 8.7 by separating variables so that

$$\nabla \cdot \vec{u}_{hor} = -\frac{i\sigma}{gh} \Phi'$$

or more correctly

$$\frac{i\sigma}{4a^2\Omega^2} F[\Theta_n] = -\frac{i\sigma}{gh_n} \Theta_n. \tag{9.18}$$

For each σ and s we have an infinitude of north-south modes- each with an equivalent depth, h_n, exactly analogous to our earlier example. Equation 9.18 is *Laplace's tidal equation.* It defines an eigenfunction-eigenvalue problem

where the equivalent depths are the eigenvalues and the eigenfunctions are known as Hough functions. Hough functions play a major role in meteorology and oceanography – representing as they do very general classes of oscillations including gravity waves, Rossby waves, and mixtures.

Solving Equation 9.18 is a technical task which we will skip over. (Details may be found in Chapman and Lindzen, 1970) We will, instead, look at the counterpart of Equation 9.18 for simpler geometries, in order that we may understand results obtained with Equation 9.18. For the moment we should note that all information about geometry and rotation is contained in h_n.

9.3.2 Vertical structure equation

Formally, the equation for z^* dependence will be the same regardless of geometry. Substituting (9.18) into (9.10) and (9.12) (and expanding J, w^*, and Φ' in terms of $\Theta_n(\theta)$) we get

$$-\frac{i\sigma}{gh_n}\Phi'_n + \frac{dw^*_n}{dz^*} - w^*_n = 0 \tag{9.19}$$

$$i\sigma\frac{d\Phi'_n}{dz^*} + w^*_n R\left(\frac{dT_0}{dz^*} + \frac{RT_0}{c_p}\right) = \kappa J_n, \tag{9.20}$$

from which Φ'_n is readily eliminated to give

$$\frac{d^2w^*_n}{dz^{*2}} - \frac{dw^*_n}{dz^*} + w^*_n\frac{R}{gh_n}\left(\frac{dT_0}{dz^*} + \frac{RT_0}{c_p}\right) = \frac{\kappa J_n}{gh_n}. \tag{9.21}$$

If we let

$$w^* = \tilde{w}e^{z^*/2}, \tag{9.22}$$

(9.21) becomes

$$\frac{d^2\tilde{w}_n}{dz^{*2}} + \left\{\underbrace{\frac{R}{gh_n}\left(\frac{dT_0}{dz^*} + \frac{RT_0}{c_p}\right)}_{\frac{1}{h_n}\left(\frac{dH}{dz^*}+\kappa H\right)} - \frac{1}{4}\right\}\tilde{w}_n = \frac{\kappa J_n}{gh_n}e^{-z^*/2}. \tag{9.23}$$

Using (9.19), our l.b.c. (i.e., lower boundary condition), (9.6) becomes

$$\frac{dw_n^*}{dz^*} + \left(\frac{H(0)}{h_n} - 1\right) w_n^* = 0 \text{ at } z^* = 0, \tag{9.24}$$

or

$$\frac{d\tilde{w}_n}{dz^*} + \left(\frac{H}{h_n} - \frac{1}{2}\right) \tilde{w}_n = 0 \text{ at } z^* = 0. \tag{9.25}$$

Again our upper boundary condition is a radiation condition. Note the following:

(a) From (9.22) we see that vertically propagating waves increase in amplitude with height in such manner as to leave energy density constant.

(b) The higher a given thermal forcing ($\rho J \sim$ constant) is applied the greater the response every place. (You have an exercise on this.)

(c) The equivalent depth of the atmosphere is the eigenvalue of Equations 9.25, 9.23 (with $J = 0$), and the upper boundary condition. As an exercise you will show that when $T_0 =$ constant, there is only one atmospheric equivalent depth, $h = \gamma H$.

(d) The equivalent depth of a mode determines the vertical wavenumber.

9.3.3 Simplified Laplace's tidal equation

Let us now look at the counterpart of Laplace's tidal equation on a rotating planar channel. Our equations for horizontal motion are (assuming solutions of the form $e^{i(\sigma t + kx)}$)

$$i\sigma u' - fv' = -ik\Phi' \tag{9.26}$$

$$i\sigma v' + fu' = -\frac{\partial \Phi'}{\partial y}, \tag{9.27}$$

where

$$v' = 0 \text{ at } y = 0, L.$$

From (9.26) and (9.27)

$$u' = \frac{\sigma k \Phi' - f \frac{\partial \Phi'}{\partial y}}{(f^2 - \sigma^2)} \tag{9.28}$$

$$v' = \frac{ikf\Phi' - i\sigma \frac{\partial \Phi'}{\partial y}}{(f^2 - \sigma^2)} \tag{9.29}$$

$$\nabla \cdot \vec{u}'_{hor} = \frac{\partial u'}{\partial x} + \frac{\partial v'}{\partial y} = \frac{-i\sigma}{(f^2 - \sigma^2)} \left\{ \frac{\partial^2 \Phi'}{\partial y^2} - k^2 \Phi' \right\} \tag{9.30}$$

'Laplace's tidal equation' becomes

$$\frac{-i\sigma}{f^2 - \sigma^2} \left\{ \frac{\partial^2 \Theta_n}{\partial y^2} - k^2 \Theta_n \right\} = -\frac{i\sigma}{g h_n} \Theta_n$$

or

$$\frac{d^2 \Theta_n}{dy^2} + \left\{ \frac{f^2 - \sigma^2}{g h_n} + k^2 \right\} \Theta_n = 0, \tag{9.31}$$

where

$$\frac{d\Theta_n}{dy} - \frac{kf}{\sigma} \Theta_n = 0 \text{ at } y = 0, L. \tag{9.32}$$

If we write

$$\Theta_n = \sin \ell y + A \cos \ell y$$

then (9.32) becomes

$$\ell \cos \ell y - A\ell \sin \ell y - \frac{kf}{\sigma} \sin \ell y - A \frac{kf}{\sigma} \cos \ell y = 0, \ y = 0, L,$$

which in turn implies

$$A = \frac{\sigma \ell}{kf}$$

and

$$\sin \ell y = 0 \text{ at } y = L,$$

or

$$\ell_n = \frac{n\pi}{L}.$$

Equation 9.31 now gives us an expression for h_n:

$$-\ell_n^2 - \left\{ \frac{f^2 - \sigma^2}{gh_n} + k^2 \right\} = 0,$$

or

$$gh_n = \frac{\sigma^2 - f^2}{k^2 + (\frac{n\pi}{L})^2}. \tag{9.33}$$

Note the following:

(a) If we set $f = 0$ and $n = 0$, we recover our earlier results for internal gravity waves (restricted by hydrostaticity – but extended to a deep fluid).

(b) h_n is positive only if $\sigma^2 > f^2$; if $\sigma^2 < f^2$, h_n is negative.

(c) From Equation 9.23 (known as the vertical structure equation) we see that negative h_n is associated with vertical trapping. What this means, physically, is that at long periods, geostrophic balances are established faster than the oscillatory cross isobaric response.

Recalling our earlier discussion of the vertical structure equation, note that h_n determines the vertical wavelength of a given mode

$$\begin{aligned} m^2 &\approx \frac{1}{h_n H}\left(\frac{1}{H}\frac{dH}{dz^*} + \kappa\right) - \frac{1}{4H^2} \qquad (9.34) \\ &\approx \frac{\kappa}{h_n H} - \frac{1}{4H^2} \text{ for an isothermal basic state,} \\ VWL &\equiv \frac{2\pi}{m}. \end{aligned}$$

Figures 9.24 and 9.25 from Lindzen (1967) show the relation between h_n and VWL (vertical wavelength). From (9.33) we see that h_n (and hence VWL) decreases as n increases (and/or L decreases).

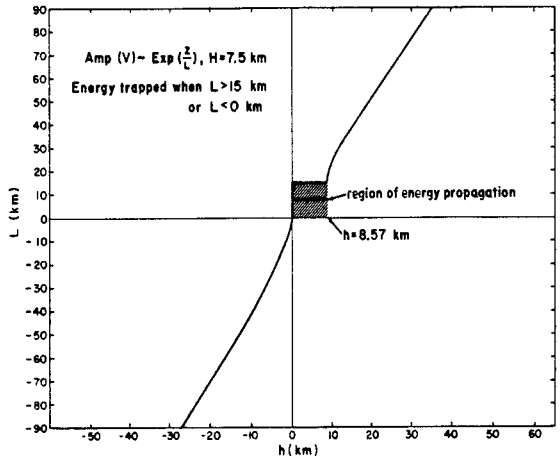

Figure 9.24: Energy trapping as a function of equivalent depth (see text for details). After Lindzen (1967).

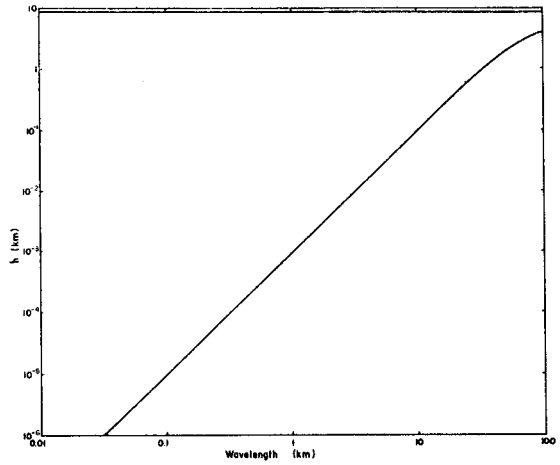

Figure 9.25: Vertical wavelength as a function of equivalent depth. After Lindzen (1967).

9.3.4 Overall procedure

Finally, we must return to tides. The following flow chart reviews our procedure.

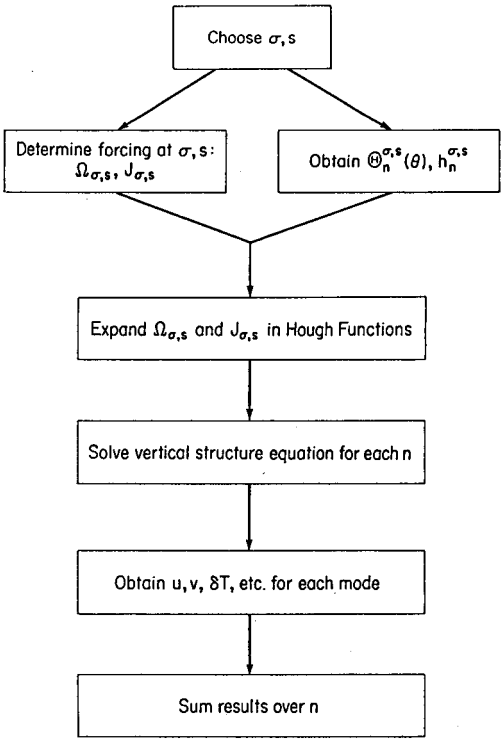

The questions we wish to focus on are:

1. Why is the semidiurnal surface pressure oscillation stronger and more regular than the diurnal oscillation?

2. Can we account for the specific observed magnitudes and structures?

In addition, we will take a brief look at the lunar tides – not because they are important *per se*, but because they tell us something very significant about how the atmosphere responds to forcing. We note here, for reference

purposes, that the only effect of gravitational forcing on our equations is to modify the lower boundary condition

$$\frac{d\tilde{w}_n}{dz^*} + \left(\frac{H}{h_n} - \frac{1}{2}\right)\tilde{w}_n = \frac{i\sigma}{gh_n}\Omega_n \quad \text{at } z^* = 0, \tag{9.35}$$

where Ω_n is a tidal contribution to the gravitational potential.

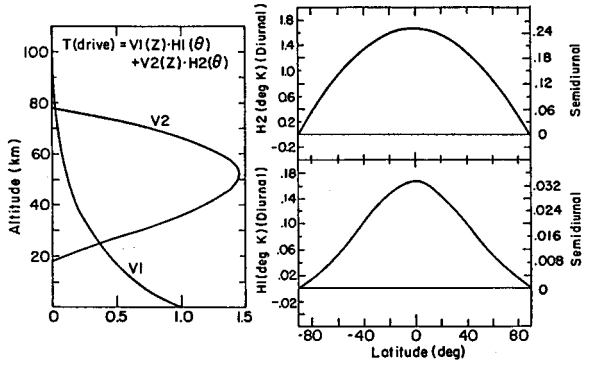

Figure 9.26: Vertical distributions of thermal excitation due to water vapor (V1) and ozone (V2); latitude distributions for water vapor (H1) and ozone (H2). After Lindzen (1968).

The thermal forcing for diurnal and semidiurnal tides is shown in Figure 9.26. It is expressed in terms of

$$T = \frac{\kappa J}{i\sigma R}. \tag{9.36}$$

This is the temperature amplitude that would be produced by J in the absence of dynamics. For the diurnal component, T is maximum at 1800 LT, while for the semidiurnal component T has maxima at 0300 and 1500 LT.

9.3.5 Semidiurnal and diurnal solutions – Hough functions

The Hough functions for the semidiurnal tide are shown in Figure 9.27; those for the diurnal tide are shown in Figure 9.28; the equivalent depths are shown in Table 9.1. Notice that the Hough functions for S_2 smoothly span the globe. The main mode resembles the latitude structure of the forcing and has an equivalent depth, 7.85 km, which is associated with either an almost infinite

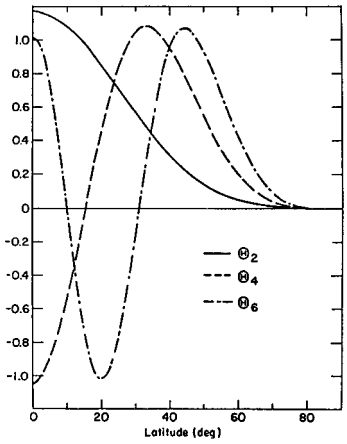

Figure 9.27: Latitude distribution for the first three symmetric solar semidiurnal migrating Hough functions. After *Chapman and Lindzen (1970).*

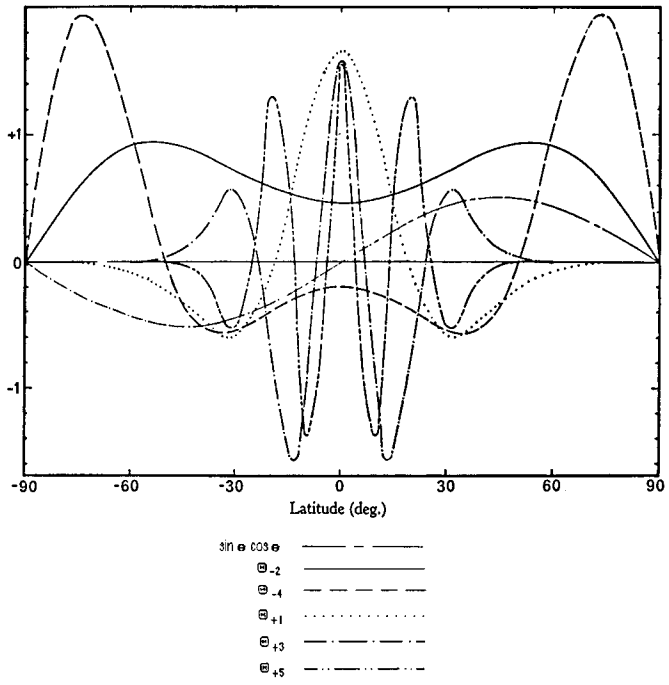

Figure 9.28: Symmetric Hough functions for the migrating solar diurnal thermal tide. Also shown is $\sin\theta\cos\theta$, the most important odd mode. After Lindzen (1967).

VWL or, sometimes, mild trapping. If we expand the heating functions we get

$$H_{0_3}^{S-D} = 0.25^\circ\mathrm{K}\Theta_2^{S-D} + 0.065^\circ\mathrm{K}\Theta_4^{S-D} + 0.036^\circ\mathrm{K}\Theta_6^{S-D} + \ldots \tag{9.37}$$

$$H_{\mathrm{H_2}0}^{S-D} = 0.031^\circ\mathrm{K}\Theta_2^{S-D} + 0.008^\circ\mathrm{K}\Theta_4^{S-D} + 0.0045^\circ\mathrm{K}\Theta_6^{S-D} + \ldots, \tag{9.38}$$

that is, the forcing primarily excites Θ_2^{S-D}. The situation for S_1 is very different indeed. Here we see two distinct sets of eigenfunctions: one concentrated in latitudes poleward of 30° latitude with negative equivalent depths and one concentrated equatorward of 30° with small positive equivalent depths. Our previous discussion enables us to understand these results. From (9.33) we see that negative (positive) equivalent depths are associated with $\sigma^2 < f^2 (\sigma^2 > f^2)$.

Table 9.1

Diurnal Mode #	h_n	Semidiurnal Mode #	h_n
+ 1	.69 km	2	7.85 km
+ 3	.12 km	4	2.11 km
+ 5	.05 km	6	0.96 km
- 2	-12.27 km		
- 4	-1.76 km		

On a sphere we have

$$f = 2\Omega \sin\phi$$

and for S_1, $\sigma = \Omega$. Therefore

$$\sigma = f$$

when

$$\sin\phi = \frac{1}{2},$$

or

$$\phi = 30^\circ.$$

Reference to Equation 9.33 makes clear what is going on. Global modes are formed such that poleward of 30° negative equivalent depth modes oscillate meridionally (real ℓ) and equatorward of 30° they decay exponentially (imaginary ℓ). The opposite situation obtains for positive equivalent depth modes. In addition, the positive (propagating) modes, being confined to the region $\mid \phi \mid < 30^\circ$, have much larger effective ℓs (meridional wavenumbers) and smaller hs than would global modes. This matter will be elucidated in an exercise.

The expansion of diurnal heating yields

$$\begin{aligned} H^D_{0_3} = \quad & 1.63^\circ\mathrm{K}\Theta^D_{-2} - 0.51^\circ\mathrm{K}\Theta^D_{-4} + \ldots \\ + \quad & 0.54^\circ\mathrm{K}\Theta^D_1 - 0.14^\circ\mathrm{K}\Theta^D_3 + \ldots \end{aligned} \tag{9.39}$$

and

$$\begin{aligned} H^D_{\mathrm{H}_2 0} = \quad & 0.16^\circ\mathrm{K}\Theta^D_{-2} - 0.055^\circ\mathrm{K}\Theta^D_{-4} + \ldots \\ + \quad & 0.062^\circ\mathrm{K}\Theta^D_1 - 0.016^\circ\mathrm{K}\Theta^D_3 + \ldots \end{aligned} \tag{9.40}$$

The above results provide an immediate answer to our first question: $S_1(p_s)$ is weaker because most of the forcing goes into trapped modes which do not effectively influence the ground. It is irregular largely because the surface response involves higher order modes which are more susceptible to regional variations. (Note that winds associated with higher order modes may even be larger.) By contrast, $S_2(p_2)$ receives almost all its forcing in a single global mode which is insensitive to regional fluctuations. Moreover, the main S-D mode has an almost infinite VWL so that all forcing contributes 'in phase'[12].

[12]On page 183 we remarked that Siebert (1961) had chosen a temperature profile which suppressed the propagation of the semidiurnal wave excited by ozone heating. What Siebert did was to choose a distribution of T_0 such that $\frac{dH}{dz^*} + \kappa H =$ constant (*viz.* Equation 9.23). Such a T_0 decreases with height in the troposphere – reasonably enough.

With respect to the second question we obtain $S_2(p_s) \sim 1.1$ mb (with two thirds of this coming from 0_3) with maxima at 0900 and 2100 LT. The amplitude is about right but the observed maxima occur at 0940 and 2140 LT. For $S_1(p_s)$, it is more useful to look at the Hough decomposition

$$\begin{aligned} S_1^{H_2 0}(p_s) = \quad & \{137\Theta_{-2}^D - 68\Theta_{-4}^D + \ldots \\ + \quad & 117e^{56^\circ i}\Theta_1^D - 13e^{73^\circ i}\Theta_3^D + \ldots\}e^{i(\Omega t+\phi)}\mu\text{b} \end{aligned} \tag{9.41}$$

$$\begin{aligned} S_1^{0_3}(p_s) = \quad & \{44\Theta_{-2}^D - 3.4\Theta_{-4}^D + \ldots \\ + \quad & 94e^{13^\circ i}\Theta_1^D - 3.75e^{16^\circ i}\Theta_3^D + \ldots\}e^{i(\Omega t+\phi)}\mu\text{b} \end{aligned} \tag{9.42}$$

The sum of Equations 9.41 and 9.42 reasonably accounts for observations. Note the relative suppression of trapped modes. Overall, the largest contributor to $S_1(p_s)$ is the ineffectively excited first propagating mode. Note also that at least three modes are of comparable importance.

We will not go into a detailed discussion of the theoretical results for upper air fields, but Figures 9.19 and 9.20 show remarkable agreement between theory and observation. Note that phase variation with height, which is evident at 20° latitude, is virtually absent at 60° latitude (Why?). Figure 9.29 shows theoretical results for semidiurnal northerly velocity oscillations. A comparison with Figure 9.18 shows compatibility with observed magnitudes but the theory predicts a 180° phase shift near 28 km while it is observed at much greater heights. Interestingly, both this discrepancy and that in the phase of $S_2(p_s)$ led to the recognition that an additional important source of tidal forcing arises from the daily variations in tropical rainfall (Lindzen, 1978).

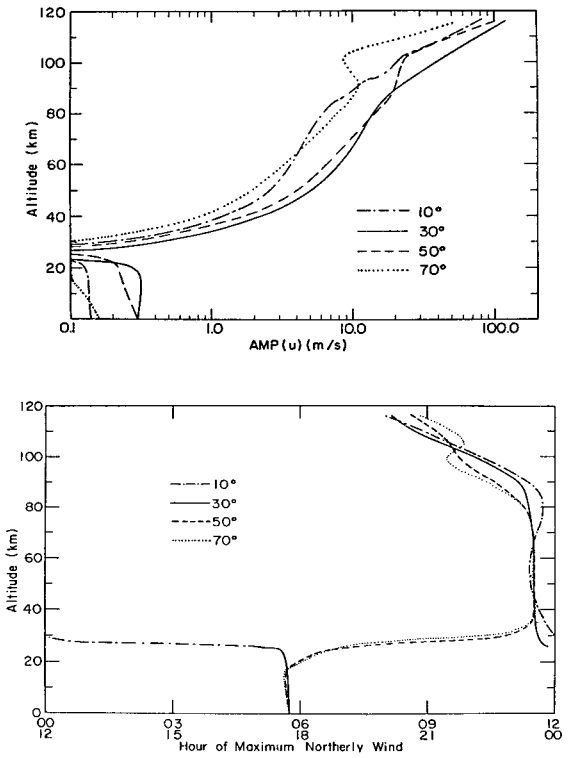

Figure 9.29: (*Top*) Amplitude of the solar semidiurnal component of u at various latitudes: equatorial standard atmosphere is used for $T_0(z)$. (*Bottom*) Phase (hour of maximum) of the solar semidiurnal components of u at various latitudes. After Lindzen (1968).

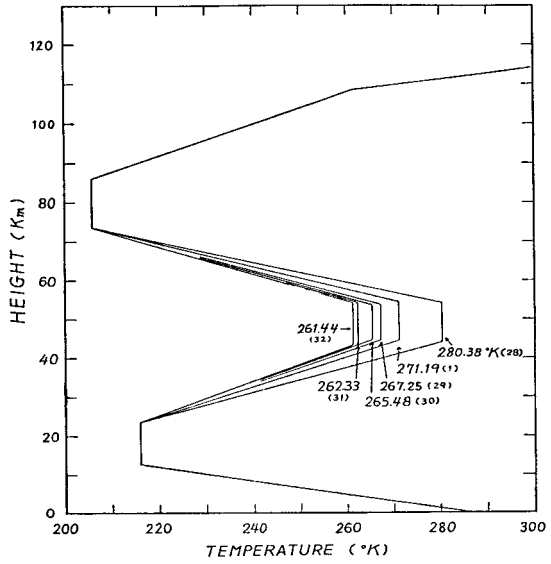

Figure 9.30: Various temperature profiles used in calculating the lunar semidiurnal surface pressure oscillation. The maximum temperature of the statopause and a profile number are shown for each of the profiles. After Sawada (1956).

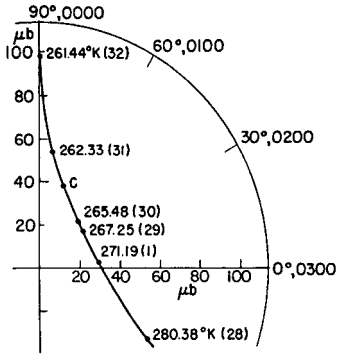

Figure 9.31: A harmonic dial for the lunar semidiurnal surface pressure oscillation. Amplitude and phase are shown as functions of the basic temperature profile. After Sawada (1956).

9.3.6 Lunar semidiurnal tide

Finally, we turn briefly to the lunar tide $L_2(p_s)$. Its Hough functions are much like those for S_2. The equivalent depth of its main mode is 7.07 km. Recall that for an isothermal basic state the atmosphere has a single equivalent depth, $h = \gamma H \approx 11$ km, which is far from resonance for the main semidiurnal modes. However, for $h \sim 7$ km we see from Equation 9.23, the vertical structure equation, that the local vertical wavenumber hovers around zero, and varies with height; there is a turning point near 60 km. Thus, as we noted, additional equivalent depths might exist and resonance might be possible (remember the behaviour of a fluid with a lid). This possibility has, in fact, been dismissed too casually. Theoretically, one finds that one can predict the observed $L_2(p_s)$ with an isothermal basic state, but Sawada (1956) found that for different basic T_0s, shown in Figure 9.30, responses shown in Figure 9.31 were obtained. Such extreme variability is certainly characteristic of resonance. Now two points must be made

(a) No such sensitivity is found for the thermally forced tides; and

(b) No such extreme variability is observed for $L_2(p_s)$. So what is happening? First, resonance of an internal wave requires that a wave travel up and down at least several times between the ground and a turning point in such a manner as to produce coherent interference. This is possible for forcing at a single level – but not for a distributed thermal excitation. (Think back to the resonance exercises at the end of Chapter 8.) Even, however, with forcing at the ground, the surface constituting the turning point must be horizontal. In reality, the basic temperature varies with latitude and coherent reflections are difficult to achieve. This shows, rather generally, the very unlikely nature of internal wave resonance in geophysical systems. A thorough analysis of this is given in Lindzen and Hong (1974).

However, the profile approaches asymptotically to a very cold constant temperature above the troposphere. This cold temperature leads to m^2 being significantly negative – as opposed to being almost zero (*viz.* Equation 9.34). Thus ozone forcing is prevented from affecting the surface pressure. Butler and Small (1963) used a realistic profile for T_0 which does not have this problem.